Coupling of flexural and longitudinal wave motion in a finite periodic structure with asymmetrically arranged transverse beams

Friis, Lars; Ohlrich, Mogens

Published in:
Journal of the Acoustical Society of America

Link to article, DOI:
10.1121/1.2126928

Publication date:
2005

Document Version
Publisher's PDF, also known as Version of record

Coupled flexural-longitudinal wave motion in a finite periodic structure with asymmetrically arranged transverse beams

Lars Friis[a] and Mogens Ohlrich[b]
Acoustic Technology, Ørsted•DTU, Technical University of Denmark, Building 352, DK-2800 Kgs. Lyngby, Denmark

(Received 17 February 2005; revised 26 September 2005; accepted 26 September 2005)

A companion paper [J. Acoust. Soc. Am. **118**, 3010–3020 2005] has examined the phenomena of flexural-longitudinal wave coupling in a practically undamped and semi-infinite periodic waveguide with structural side-branches. The effect of structural damping on wave coupling in such a waveguide is examined in the first part of the present paper, and the damping-dependent decrease in wave coupling is revealed for a structure with multiresonant side-branches. In the second part, the simplifying semi-infinite assumption is relaxed and general expressions for the junction responses of *finite* and *multicoupled* periodic systems are derived as a generalization of the governing expressions for finite, mono-coupled periodic systems [Ohlrich, J. Sound Vib. **107**, 411–434 (1986)]. The present derivation of the general frequency response of a finite system utilizes the eigenvectors of displacement responses and wave forces that are associated with the characteristic wave-types, which can exist in a multicoupled periodic system [Mead, J. Sound Vib. **40**, 19–39 (1975)]. The third part of the paper considers a finite specific test-structure with eight periodic elements and with structural terminations at the extreme ends. Audio-frequency vibration responses of this tri-coupled periodic structure are predicted numerically over a broad range of frequencies and a very good agreement is found with the measurement results obtained from an experiment with a nominally identical, periodic test-structure which is freely suspended. [DOI: 10.1121/1.2126928]

PACS number(s): 43.40.At, 43.40.Cw, 43.20.Bi [MO] Pages: 3607–3618

I. INTRODUCTION

Flexural-longitudinal wave coupling in a periodic waveguide with structural side-branches was examined in a companion paper.[1] For a specific choice of side-branches in the form of relatively short transverse beams attached at regular intervals the coupling phenomena were clearly demonstrated, and it was found that the long-range transmission of structural wave motion was significantly enhanced in broad frequency bands due to this wave coupling between flexural and longitudinal motion. Such coupled motion in spatially periodic structures can be "provoked" in various ways but is most often a result of geometrical asymmetry as is the case for rib-stiffened plates or building columns with beams and floors attached at regular intervals as in multi-story buildings. A simple model of such a transmission path is shown in Fig. 1 as a periodic assembly of beam-type components, or as an idealized plane-wave, normal incidence model of a similar plate assembly; the transverse beams are attached asymmetrically—to one side only—on an otherwise continuous waveguide, that is, a continuous beam, column or plate structure. It is this type of *asymmetrical* periodic structure that is the subject of the present investigation.

The wave propagation characteristics of a practically *undamped* and *semi-infinite* periodic structure of this type were examined in Ref. 1. Numerical results for a system with relatively short-length transverse beams ($l_t = l/8$), which were still resonant within the frequency range considered, showed that the flexural-longitudinal wave coupling has a drastic effect on the wave propagation properties in comparison to those of a corresponding system with *symmetrically* attached cross beams, which are known to generate significant broadband attenuation of flexural waves.[2] Although the asymmetrical system[1] was excited by an external point moment—that was anticipated to excite a predominantly flexural wave, which is governed by a broad "stopband" at mid-frequencies—the inherent wave coupling resulted in a highly enhanced wave transmission with very little attenuation of flexural motion from element to element. This enhanced transmission is caused by another wave-type, which is predominantly longitudinal and propagates with significant components of both flexural and longitudinal displacements. So, the wave conversion implies that both flexural and longitudinal wave-energies are transported by *whichever* wave-type that is able to propagate, and that wave transmission is only effectively reduced in frequency bands where *all* the wave-types present are sufficiently attenuated. Whether this also applies for periodic structures with extended (long) and multiresonant side-branches and for systems with typical values of structural damping (as opposed to undamped systems) is examined in this paper. An understanding of this type of transmission path is of considerable practical interest, for example, in the prediction of structureborne sound transmission in web-stiffened panels, in ship hulls that have decks to one side only, and in supporting column-structures in building-skeletons.

[a]Electronic mail: lf@oersted.dtu.dk
[b]Electronic mail: mo@oersted.dtu.dk

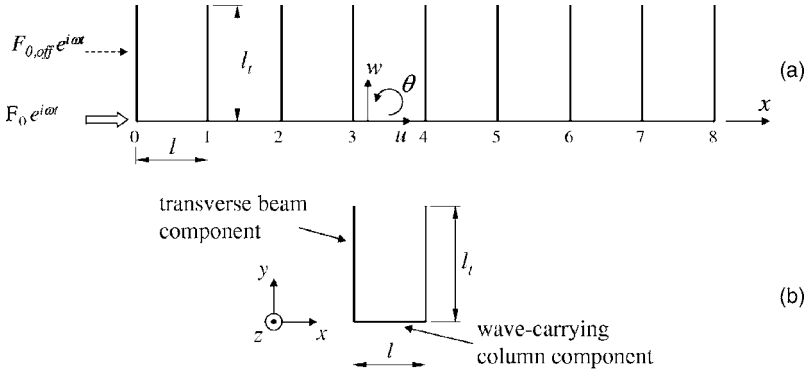

FIG. 1. (a) Periodic structure with asymmetrical side-branches in the form of transverse beams; (b) corresponding periodic element that is symmetrical with respect to its center $x=l/2$.

Periodic structures have been studied for many years but only a few authors have considered the problem of wave coupling and the effect of structural damping thereon. In an experimental investigation Gösele[3] measured the structure-borne sound transmission in a model structure representing the outer wall and flanking columns of a building structure, which was loaded asymmetrically with thick floor plates, causing a significant characteristic mobility-mismatch in the order of 1:70. It was shown that stiffening of the wall by two flanking columns significantly enhanced the wave transmission, as vibrational energy was transported through the columns rather than the wall. Presumably flexural-longitudinal wave coupling or flexural-torsional wave coupling or combinations thereof caused this. Mead and Markus[4] studied flexural-longitudinal wave coupling in a simple multisupported beam loaded eccentrically with single degree-of-freedom oscillators on levers, and they demonstrated that a *high value* of structural damping in the wave-carrying beam resulted in a very substantial decrease in the coupling between flexural and longitudinal motions. Whether such a decrease occurs in a moderately damped engineering structure like that sketched in Fig. 1 is examined in the present paper.

A. Fundamental relations for periodic structures

Periodic structure theory is briefly summarized in a companion paper,[1] so it is only the most basic relations that will be given here. Wave propagation in infinite periodic structures can be determined from knowledge of the dynamic properties of just a single "periodic element." Consider harmonic wave motion in an undamped and infinite periodic structure composed of repeated elements that are coupled with one another through the smallest possible number of motion coordinates n. The response of such a structure is governed by n characteristic free, harmonic wave-types, which can exist simultaneously and independently at any frequency.[5–7] These wave-types occur in n pairs of positive and negative-going waves, with the corresponding propagation characteristics being described by a pair of complex and frequency-dependent characteristic "propagation constants" $\mu=\pm(\mu_R+i\mu_I)$. Usually, μ_R is called the "attenuation constant" and μ_I the "phase constant;" both quantities are defined as being positive. So, if only a single positive-going characteristic harmonic wave with propagation constant μ and angular frequency ω travels through the system, then the complex displacements $q(x)=q(\xi)$ and $q(\xi+l)$ at identical positions ξ in adjacent elements of length l are related by $q(\xi+l)e^{i\omega t}=e^{\mu}q(\xi)e^{i\omega t}$. Hence, if the solution of μ takes on negative values the wave is progressing in the positive direction. These relationships show that free wave motion is possible only in frequency bands where μ is purely imaginary, that is, $\mu=\pm i\mu_I$. These bands are known as "propagation zones" or "passbands." For negligible structural damping a wave thus propagates throughout the system without change in amplitude. The frequency bands in which μ is real, that is, $\mu=\pm\mu_R$ or $\mu=\pm\mu_R\pm i\pi$, are called "attenuation zones" or "stopbands," since no transport of vibrational energy is possible and the wave amplitude is attenuated (reduced) from element to element.

B. Background and outline of paper

The paper examines wave propagation and response in asymmetrical periodic structures of the type shown in Fig. 1, which exemplifies a tri-coupled periodic structure with multiresonant point loadings caused by continuous cross-members (or side-branches). Damping loss factors in building structures, for example, typically take values in the range of 0.01–0.05, and this cannot be neglected in a prediction of wave transmission. The influence of structural damping on wave propagation and flexural-longitudinal wave coupling in a semi-infinite periodic structure is therefore examined numerically in Sec. II by using the expression derived in a companion paper.[1] The simplifying assumption behind the use of *infinite* or *semi-infinite* periodic systems is well justified for such analyses of wave propagation phenomena. However, most engineering structures consist of a relatively small number of periodic elements, which are only moderately damped. This means that reflections from the ends of a periodic system cannot be ignored and the system thus has to be treated as a *finite* periodic system, which, for a multicoupled periodic system, complicates the analysis considerably. A derivation of the frequency response functions of such finite periodic structures is of course very important, but has not been done before to the authors' knowledge.

Section III therefore presents an extensive derivation of a general expression for the junction-response of *finite* and *multicoupled* periodic systems. This is derived as a generalization of the governing expression for finite, *mono-coupled* periodic systems.[8] Together with a set of generalized wave coordinates the present derivation also utilizes the eigenvectors of displacements and wave forces that are associated with the characteristic wave-types, which can exist in a multicoupled periodic system;[9] the present analysis is based on

the receptance approach to the periodic structure theory.[7,9,10] Basically, this approach utilizes that harmonic displacements and forces at the terminals of a single periodic element are related by its dynamic receptances—or mobilities if these are preferred. With the harmonic time variation omitted, and by denoting the left- and right-hand ends of a periodic element by indices l and r, respectively, these relations between displacements q and forces F read $q_l=\alpha_{ll}F_l+\alpha_{lr}F_r$ and $q_r=\alpha_{rl}F_l+\alpha_{rr}F_r$, where α_{ll} and α_{rr} are the direct receptances of the periodic element and α_{lr} and α_{rl} are the transfer receptances. Now, relationships between displacement amplitudes in adjacent periodic elements and between corresponding forces were given in Sec. I A; evaluating these at the left- and right-hand ends of a single periodic element yield $q_r=e^{\mu}q_l$ and $F_r=-e^{\mu}F_l$. So, by substitution, the propagation constant μ is readily expressed in terms of the element receptances.[1]

Finally, in Sec. IV the derived junction-receptance is put into use in response predictions of a specific test-structure with eight periodic elements and with structural terminations at the extreme ends. Audio-frequency vibration responses of this tri-coupled periodic structure are predicted numerically over a broad range of frequencies and the results are compared with experimental measurements on a nominally identical periodic test-structure.

II. NUMERICAL INVESTIGATION OF THE EFFECT OF DAMPING

A wave analysis and numerical parameter study have been conducted for investigating the effect of structural damping on wave coupling and response of asymmetrical periodic structures that undergo flexural and longitudinal vibration. We consider a *semi-infinite* periodic structure similar to that depicted in Fig. 1, albeit extending toward infinity in the positive x-direction. This free or semidefinite system is driven by an external forcing vector $\mathbf{F}_0e^{i\omega t}$ that represents both longitudinal and transverse force excitations as well as moment excitation. Note that application of any *single one* of these force components will generate a *coupled* or *mixed* response comprising both longitudinal and flexural motions because of the structural asymmetry. The vibration response of the wave-carrying components (and elsewhere) is governed by *three* motion degrees-of-freedom, comprising displacements $u(x,t)$, $w(x,t)$, and $\theta(x,t)$ in the longitudinal, transverse, and rotational directions.

The *periodic element* of the structure, shown in Fig. 1(b), consists of a wave-carrying beam or column component of length l, and two multiresonant load components in the form of transverse beams of length l_t. For convenience in analysis the periodic element is chosen to be symmetrical about the middle of the column component, which means that the element can be rotated 180° about the y axis without changing its dynamic properties. This symmetry of the periodic element is achieved by halving each transverse beam in the z direction into beams of half-width. Thus, when every second periodic element is rotated 180° about its vertical center axis and periodic elements are physically connected to one another, then the transverse beams of half-width become sideways interconnected to form transverse beams of full width.

The structural properties and dimensions of the components used in the present simulations are identical to those used in the predictions and experimental investigation in Sec. IV. The wave-carrying component has length $l=235$ mm, thickness $h=15$ mm, and width $b=20$ mm, whereas the appended transverse beam has length $l_t=380$ mm (i.e., $l_t\approx 1.6\cdot l$), thickness-parameter $h_t=h$, and width-parameter $b_t=b$. The structure is made of acrylic with Young's modulus $E=5.4\cdot 10^9$ N/m^2 and density $\rho=1200$ kg/m^3. Material damping is modeled by letting Young's modulus become complex as $\underline{E}=E(1+i\eta)$, where η is the damping loss factor. Calculations have been made for three values of damping loss factor η, namely 0.001, 0.01, and 0.056, where the high value is identical to the experimentally determined loss factor for an acrylic test beam sample.

The semi-infinite structure considered is similar to the one investigated in a companion paper,[1] except for dimensions of the transverse beam components. Hence, the expressions used in the present numerical simulations for calculating the required quantities like element receptances, propagation constants, associated force and displacement vectors, energy ratios and vibration responses, can all be found in Ref. 1 and will not be repeated here. It should be mentioned that the element's components are modeled using Bernoulli-Euler beam theory, albeit with correction for shear deformation,[11] and that the computations have been done using MATLAB.

A. Propagation constants

Since the periodic structure is tri-coupled, asymmetrical, and semi-infinite, its response thus results from the sum of contributions from three positive-going characteristic waves, which all include components of the displacements $u(x,t)$, $w(x,t)$, and $\theta(x,t)$. The wave-field in each wave-carrying beam component is of course composed of both positive and negative-going waves; these waves result in the positive-going characteristic waves. Note that for the finite system studied later on, one also has to include three corresponding negative-going characteristic waves due to reflections from boundaries. Accordingly, the waves-types in the periodic structure are associated with three pairs of propagation constants $\mu_i=\pm(\mu_{i,R}+\mu_{i,I})$ where $i=A,B,C$. Here $\mu_{i,R}$ and $\mu_{i,I}$ are defined as positive and thus the three positive-going waves are associated with the values $\mu_{i,+}=-\mu_i=-(\mu_{i,R}+i\mu_{i,I})$, (and the three negative-going waves are associated with $\mu_{i,-}=\mu_i=\mu_{i,R}+i\mu_{i,I}$).

The calculated wave characteristics for the semi-infinite structure are presented in Fig. 2. This shows the frequency variation of the real and imaginary parts of the propagation constants, that is, the attenuation constants μ_R and the phase constants μ_I, associated with the three pairs of wave-types. In Fig. 2(a) results are shown for a very low damping value of $\eta=0.001$; this shows that for frequencies above 35 Hz one wave-type, say type C, is governed by a very high attenuation constant and this wave can thus be regarded as a flexural near-field.[1] The two other wave-types, say A and B, which

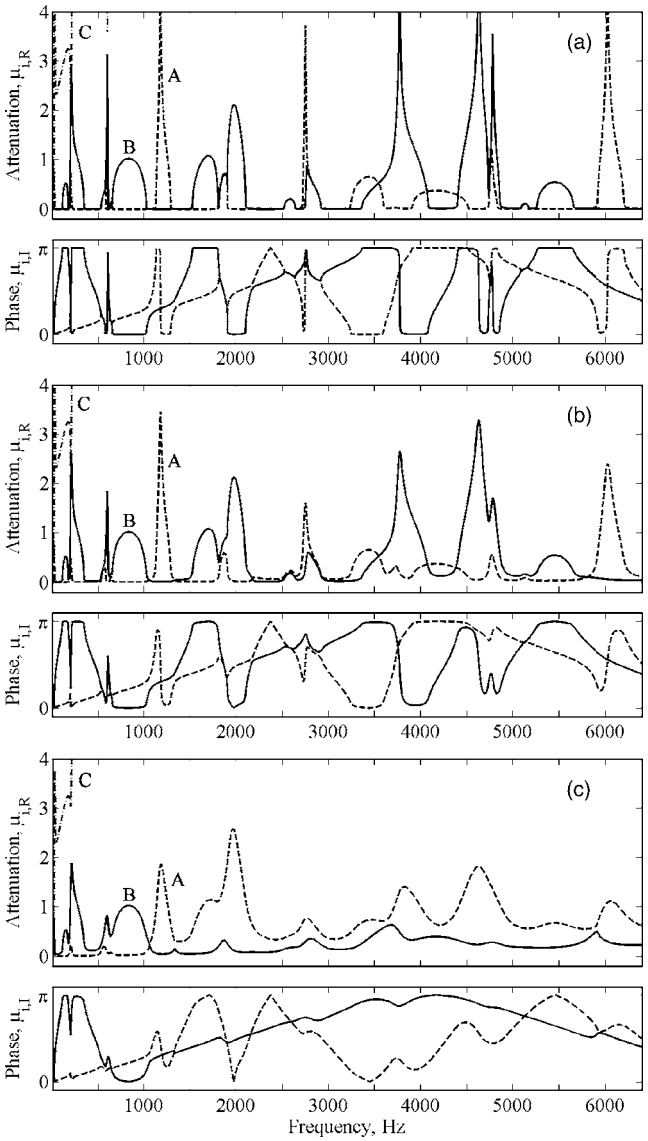

FIG. 2. Frequency variation of the real and imaginary parts of the propagation constants $\mu_i=\mu_{i,R}+\mu_{i,I}$ for the three wave-types: (---) flexural-longitudinal wave *A*; (—) flexural-longitudinal wave *B*; (--·) predominantly flexural near-field *C*. Damping loss factors: (a) $\eta=0.001$; (b) $\eta=0.01$; (c) $\eta=0.056$.

alternate between being either propagating or attenuated, must be regarded as being of both longitudinal and flexural nature. The very complicated pattern of propagation zones and attenuation zones shown here are to a large extent caused by the various modes of the transverse beams; the occurrence of both smooth and resonant type attenuation zones is explained in detail in Ref. 1. Still, it should be mentioned that no direct *crossing* of the phase constants of wave-type *A* and *B* occurs; the phase constants either (i) diverge or (ii) merge, so that the propagation constants become almost complex conjugates with nonzero attenuation constant. The first phenomenon is most pronounced at 1066, 1330, and 2175 Hz; at these frequencies the phase constant of each wave "jumps to" the slope of the other wave and the flexural-longitudinal wave coupling is found to be particularly strong. Usually the steeper phase characteristic is associated with a flexural-type wave whereas the more gradual and nearly linear phase characteristic is associated with a longitudinal-type wave. The second phenomenon occurs at several frequencies but may be seen to be most apparent in the bands around 560, 1860, 2580, 2830, 4755, and 5125 Hz. In these bands the wave with strongly coupled longitudinal-flexural motions is *attenuated* as it progresses through the periodic structure.

With a "moderate value" of structural damping of $\eta=0.01$, the results in Fig. 2(b) show that this increased damping causes a weak widening of the attenuation zones into previous propagation zones as well as a decrease in magnitude of the attenuation constants at peak attenuation frequencies. Furthermore, the attenuation constants and phase constants slightly separate in the frequency bands, which were previously assigned as complex conjugate zones in Fig. 2(a). This indicates that flexural-longitudinal wave coupling decreases when structural damping is increased, and this is clearly demonstrated in Fig. 2(c), which shows results for a damping value of $\eta=0.056$; in contrast to the results in Fig. 2(a) the phase constants are now seen to *cross-over* directly and become almost linear in certain frequency bands. This is the case in the frequency range from 0 to 1066 Hz for wave-type *A* and from 1066 Hz and upwards for wave-type *B*. As mentioned before, this almost linear phase characteristic is typically associated with a longitudinal wave. Figure 2(c) also reveals that the predominantly longitudinal wave is able to progress through the structure with relatively little attenuation in wave amplitude, since the associated attenuation constant is less than 0.3 in most parts of the frequency range considered. The predominantly flexural wave, however, which is associated with the steeper phase characteristic, is more significantly attenuated in nearly the whole frequency range.

Now, a more quantitative characterization of the wave-types than inspections of the propagation constant curves can provide, requires a determination of the displacement contributions and associated energies in the different wave-types. Such a characterization can be revealed by computing the normalized displacement vector associated with each wave-type and from this the corresponding wave energy.[1,4]

B. Nature of wave-types

The relative amounts of flexural and longitudinal motions contained in each wave-type can be quantified by the associated kinetic energy ratio ($E_{\mathrm{kin},F}/E_{\mathrm{kin},L}$), being the ratio between maximum kinetic energies of flexural and longitudinal motions in the wave-carrying column component. Figure 3 shows these energy ratio levels corresponding to the propagation constants given in Fig. 2. From Fig. 3(a), where $\eta=0.001$, it is readily seen that wave-types *A* and *B* must both be classified as being longitudinal-flexural, since each of them alternates in a complicated manner between being either predominantly longitudinal or flexural, or occasionally fully mixed, with approximately equal contributions. Wave-type *C*, however, has an energy ratio level of more than 70 dB in almost the entire frequency range and thus can be regarded as a flexural near-field. In complex conjugate zones the energy levels of the two mixed wave-types are seen to be

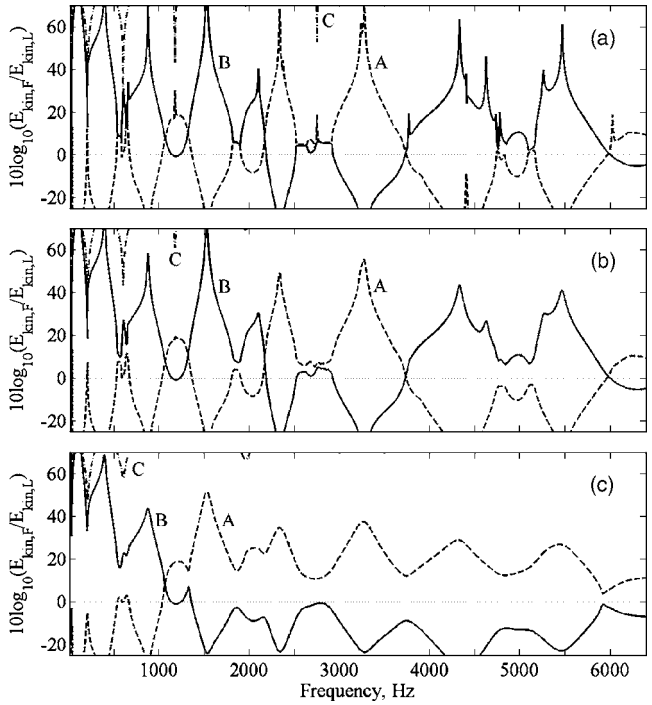

FIG. 3. Energy ratios $E_{kin,F}/E_{kin,L}$ for the three wave-types: (---) flexural-longitudinal wave A; (—) flexural-longitudinal wave B; (---) predominantly flexural near-field C. Damping loss factors: (a) $\eta=0.001$; (b) $\eta=0.01$; (c) $\eta=0.056$.

equal. The crossing of the energy ratios occurs only in the earlier mentioned regions where the phase constants of Fig. 2(a) diverge from one another.

When the loss factor is increased to $\eta=0.01$, Fig. 3(b) shows that the two mixed wave-types A and B separate in the frequency bands, which were formerly complex conjugate zones. Furthermore, peaks and troughs are smoothed especially at high frequencies. The pattern of the energy ratios, though, is the same as in Fig. 3(a), but a further *increase* of the loss factor to $\eta=0.056$ drastically changes this, as the two wave-types become almost completely separated, see Fig. 3(c). Now, the two energy ratios cross only at 1066 Hz, which is the region where the two phase constants in Fig. 2(c) diverge from one another. Consistent with earlier statements it is seen that the linear parts of the phase constants in Fig. 2(c) are associated with a predominantly longitudinal wave, whereas the steeper phase characteristic is associated with a predominantly flexural wave.

C. Junction responses

Finally the effect of damping on the response of the semi-infinite structure is investigated. For a harmonic *moment* excitation of unit magnitude Fig. 4 shows the maximum flexural displacement responses of the column component in the first eight periodic elements. For a loss factor of $\eta=0.001$, it is seen from Fig. 4(a) that flexural waves are propagating with practically no attenuation from element to element in approximately half the frequency range considered. A closer inspection reveals that some of the attenuation bands in Fig. 2(a) have little or no influence on the response. This phenomenon, which is due to flexural-longitudinal

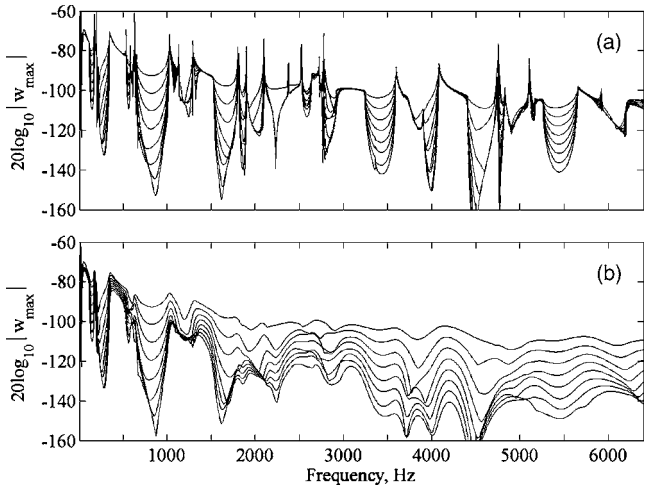

FIG. 4. Maximum transverse displacements w_{max} in column component of the first eight elements of semi-infinite periodic structure. Excitation by a harmonic point moment of unit amplitude. Damping loss factors: (a) $\eta=0.001$; (b) $\eta=0.056$.

wave coupling, is readily seen in the frequency bands around 1200, 3750, and 6000 Hz, and occurs whenever one wave-type is propagating and the other wave-type is *strongly* attenuated and their energy ratio levels in Fig. 3(a) are less than, say, 20 dB apart. Nevertheless, because of the moment excitation the predominantly flexural wave will dominate the response once the energy ratio levels are more than 20 dB apart; this evidently occur in the bands around the frequencies 150, 310, 875, 1595, 3440, 4010, 4450, and 5440 Hz. In complex conjugate zones, e.g., around 1860, 2580, and 2830 Hz, both wave-types are attenuated and the flexural responses and longitudinal responses are thus both reduced from element to element.

Figure 4(b) shows the flexural responses for a high loss factor of $\eta=0.056$. This increase of structural damping drastically affects the junction responses of the semi-infinite periodic structure; at all frequencies from about 1600 Hz and *upwards* the flexural responses are significantly reduced from element to element. This is because the flexural motion is dominated by wave-type A, which is considerably attenuated. However, in frequency bands where wave-type A is *strongly* attenuated, e.g., around 1200, 2000, and 4600 Hz, this wave becomes insignificant after just a few elements and the *less* attenuated wave-type B then takes over and dominates the flexural response of the elements that follows. Gösele[3] observed a similar wave conversion behavior and Mead and Markus[4] also discussed this phenomenon.

For a harmonic *longitudinal* unit force excitation Fig. 5 shows the maximum longitudinal displacement responses of the column component in the first eight elements. For a loss factor of $\eta=0.001$, Fig. 5(a) shows that longitudinal waves are propagating in almost the whole frequency range. Up to 3400 Hz and from 4500 Hz and upwards, this wave propagation is only interrupted by narrow bands of attenuation arising mostly from complex conjugate zones. In the frequency band from 3400 to 4500 Hz wider attenuation zones occur, as the predominantly longitudinal wave is signifi-

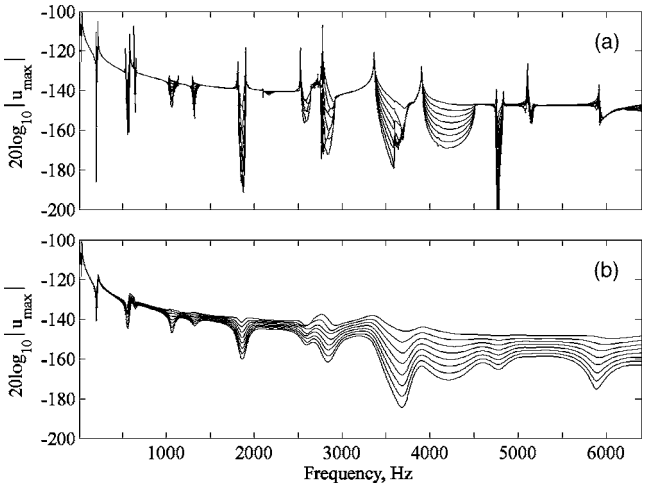

FIG. 5. Maximum longitudinal displacements u_{max} in column component of the first eight elements of semi-infinite periodic structure. Excitation by a harmonic longitudinal point force of unit amplitude. Damping loss factors: (a) $\eta=0.001$; (b) $\eta=0.056$.

cantly attenuated and the energy ratio levels in Fig. 3(a) are more than 20 dB apart.

In the present case of relatively light modal point loadings posed by the transverse beams, it can be shown that the longitudinal displacement responses—apart from minor deviations—follow closely the asymptotic response of a *simple continuous* and semi-infinite column structure of the same cross-sectional area S. Essentially, this implies that the corresponding longitudinal *velocity* responses of the system are almost independent of frequency in the range considered.

Figure 5(b) shows the longitudinal responses for the high loss factor of $\eta=0.056$. This increase of damping enhances only the attenuation slightly at higher frequencies. Furthermore, the damping enforces no particular change in the response pattern as attenuation occurs at the same frequencies as in Fig. 5(a). As the predominantly longitudinal wave-type has the lowest value of attenuation constant at all frequencies, then this is governing the longitudinal responses at all junctions of the structure.

III. FINITE PERIODIC STRUCTURES

Engineering structures that are spatially periodic often consist of relatively few periodic elements; this means that reflections from the extreme boundaries cannot be neglected and the periodic structures must therefore be treated as *finite*. Ohlrich[8] derived governing expressions for the response of finite, *mono-coupled* periodic systems in terms of the system's junction-receptances. The same derivation procedure is generalized herein and used for determining the junction-receptances of *finite* and *multicoupled* periodic systems. A general expression for a $n\times n$ junction-receptance matrix is derived for a system with arbitrary terminations. In this derivation use is also made of a wave-reflection technique developed by Mead,[9] and this was outlined and extended in the companion paper.[1]

Figure 6 shows schematically a finite system with N periodic elements and arbitrary terminations A and B at junctions O and N, respectively. These terminations may be defined by their $n\times n$ receptance matrices $\boldsymbol{\alpha}_A$ and $\boldsymbol{\alpha}_B$. It is assumed that the structure is excited at junction j by an *external* harmonic force vector $\mathbf{F}_j e^{i\omega t}$, which introduces a discontinuity. In order to determine the harmonic response at an arbitrary junction of the total system, it is expedient[8] to analyze the system as being composed of two subsystems in parallel, as shown by the block diagram in Fig. 6(b). The motions generated in each subsystem can be represented by n characteristic positive-going waves and n characteristic negative-going waves, of which each wave is associated with the propagation constants $\mu_{i,+}=-\mu_i$ and $\mu_{i,-}=\mu_i$, respectively, and where $i=1,2,3,\ldots,n$. The effect of the terminations can be taken into account by determining the corresponding reflection matrices.

A. Reflection from system boundaries

A relationship between the n waves incident on a boundary and the n waves being reflected by this is derived in the following. Consider the ith positive-going wave at angular frequency ω impinging on boundary B. This wave has the propagation constant $\mu_{i,+}=-(\mu_{i,R}+\mu_{i,I})$ and is associated with an n-element force eigenvector $\mathbf{F}_{i,B+}$ given by

$$\mathbf{F}_{i,B+}=\mathbf{f}_{i,+}\psi_{i,B+}, \tag{1}$$

where $\mathbf{f}_{i,+}$ is a *normalized force vector* with n entries and $\psi_{i,B+}$ is a *generalized wave coordinate* at boundary B. This force vector $\mathbf{f}_{i,+}$ only depends upon the receptances and propagation constants of the periodic element, whereas $\psi_{i,B+}$ is also a function of the position in the structure and the type of external excitation. The normalized force vector $\mathbf{f}_{i,+}$ is an eigenvector obtained for each wave-type as described in a

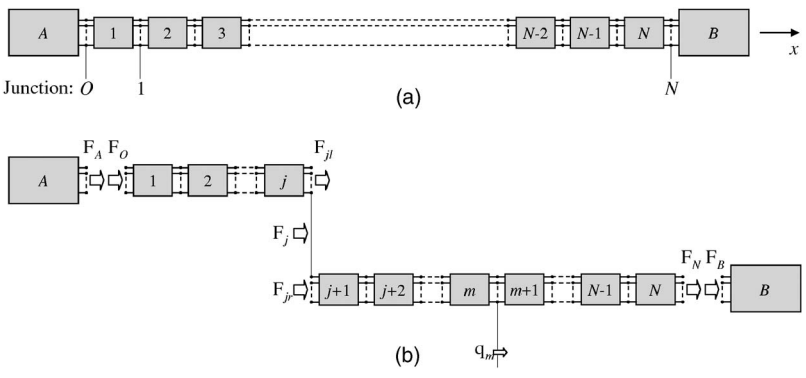

FIG. 6. (a) Block diagram of a finite multicoupled periodic structure with arbitrary terminations A and B. (b) Free body diagram for interior junction excitation.

companion paper.[1] Corresponding to the force eigenvector there is a displacement vector given as

$$\mathbf{q}_{i,B+} = \boldsymbol{\zeta}_{i,+}\psi_{i,B+}, \tag{2}$$

where $\boldsymbol{\zeta}_{i,+}$ is a *normalized displacement vector*.

The relationship between the normalized force vector $\mathbf{f}_{i,+}$ and the corresponding displacement vector $\boldsymbol{\zeta}_{i,+}$ yields[1]

$$\boldsymbol{\zeta}_{i,+} = \boldsymbol{\alpha}_{ll}\mathbf{f}_{i,+} - \boldsymbol{\alpha}_{lr}\mathbf{f}_{i,+}e^{-\mu_i}, \tag{3}$$

where $\boldsymbol{\alpha}_{ll}$ and $\boldsymbol{\alpha}_{lr}$, respectively, are the direct and transfer receptance matrices of the *periodic element*. At boundary B this particular positive-going wave causes n characteristic negative-going waves to be reflected back into the periodic system. So, if not only one but n characteristic waves impinge on the boundary B, then each of these is reflected into n negative-going waves. These $n\times n$ reflected waves form n negative-going waves, each of which consists of n wave contributions. Associated with each of these n negative-going waves there is a propagation constant μ_i, a force eigenvector $\mathbf{F}_{i,B-}$, and a corresponding displacement vector $\mathbf{q}_{i,B-}$ that are given by

$$\mathbf{F}_{i,B-} = \mathbf{f}_{i,-}\psi_{i,B-}, \quad \mathbf{q}_{i,B-} = \boldsymbol{\zeta}_{i,-}\psi_{i,B-}, \tag{4}$$

respectively. By analogy to Eq. (3) the normalized displacement vector and force vector are related as

$$\boldsymbol{\zeta}_{i,-} = \boldsymbol{\alpha}_{ll}\mathbf{f}_{i,-} - \boldsymbol{\alpha}_{lr}\mathbf{f}_{i,-}e^{\mu_i}. \tag{5}$$

Now, the total force vector $\mathbf{F}_B$ at boundary B is a sum of $2n$ force eigenvectors from n impinging waves and n reflected waves, which yields

$$\mathbf{F}_B = \sum_{i=1}^{n}\mathbf{f}_{i,+}\psi_{i,B+} + \sum_{i=1}^{n}\mathbf{f}_{i,-}\psi_{i,B-} = \mathbf{f}_+\boldsymbol{\psi}_{B+} + \mathbf{f}_-\boldsymbol{\psi}_{B-}, \tag{6}$$

where $\mathbf{f}_+$ and $\mathbf{f}_-$ are $n\times n$ element matrices containing n normalized force eigenvectors and $\boldsymbol{\psi}_{B+}$ and $\boldsymbol{\psi}_{B-}$ are column vectors containing n generalized coordinates associated with the positive and negative-going waves, respectively. In a similar manner the total displacement vector at boundary B can be expressed as a sum of contributions from n impinging and n reflected waves giving

$$\mathbf{q}_B = \sum_{i=1}^{n}\boldsymbol{\zeta}_{i,+}\psi_{B,i,+} + \sum_{i=1}^{n}\boldsymbol{\zeta}_{i,-}\psi_{B,i,-} = \boldsymbol{\zeta}_+\boldsymbol{\psi}_{B+} + \boldsymbol{\zeta}_-\boldsymbol{\psi}_{B-}, \tag{7}$$

where $\boldsymbol{\zeta}_+$ and $\boldsymbol{\zeta}_-$ are matrices with $n\times n$ entries containing normalized displacement vectors of the n positive and negative-going waves, respectively. Using Eqs. (3) and (5) these can be written as

$$\boldsymbol{\zeta}_+ = \boldsymbol{\alpha}_{ll}\mathbf{f}_+ - \boldsymbol{\alpha}_{lr}\mathbf{f}_+\mathbf{e}_d^{-\boldsymbol{\mu}}, \tag{8}$$

$$\boldsymbol{\zeta}_- = \boldsymbol{\alpha}_{ll}\mathbf{f}_- - \boldsymbol{\alpha}_{lr}\mathbf{f}_-\mathbf{e}_d^{\boldsymbol{\mu}}. \tag{9}$$

Here, the notations $\mathbf{e}_d^{-\boldsymbol{\mu}}$ and $\mathbf{e}_d^{\boldsymbol{\mu}}$ represent *diagonal matrices* containing all values of $e^{-\mu_i}$ and e^{μ_i}, respectively. The boundary condition at B is given by $\mathbf{q}_B = \boldsymbol{\alpha}_B\mathbf{F}_B$, and inserting Eqs. (6) and (7) into this gives

$$\boldsymbol{\zeta}_+\boldsymbol{\psi}_{B+} + \boldsymbol{\zeta}_-\boldsymbol{\psi}_{B-} = \boldsymbol{\alpha}_B(\mathbf{f}_+\boldsymbol{\psi}_{B+} + \mathbf{f}_-\boldsymbol{\psi}_{B-}). \tag{10}$$

This yields a relationship between the generalized wave coordinate vectors of the reflected waves $\boldsymbol{\psi}_{B-}$ and the incident waves $\boldsymbol{\psi}_{B+}$:

$$\boldsymbol{\psi}_{B,-} = -(\boldsymbol{\alpha}_B\mathbf{f}_- - \boldsymbol{\zeta}_-)^{-1}(\boldsymbol{\alpha}_B\mathbf{f}_+ - \boldsymbol{\zeta}_+)\boldsymbol{\psi}_{B+}, \tag{11}$$

where superscript -1 denotes a matrix inversion. This may be expressed in short form as

$$\boldsymbol{\psi}_{B-} = \mathbf{r}_B\boldsymbol{\psi}_{B+}, \tag{12}$$

where $\mathbf{r}_B$ is the matrix of reflection factors at boundary B.

The reflection matrix of boundary A can be found similarly by noting that the incident waves on A are negative-going and the reflected waves are positive-going. Thus, let the force vectors of the incident and reflected waves be given by

$$\mathbf{F}_{i,A-} = \mathbf{f}_{i,-}\psi_{i,A-}, \quad \mathbf{F}_{i,A+} = \mathbf{f}_{i,+}\psi_{i,A+}, \tag{13}$$

respectively. The total force vector at boundary A is a sum of force eigenvectors corresponding to n incident and n reflected waves, i.e.,

$$\mathbf{F}_A = -\mathbf{f}_+\boldsymbol{\psi}_{A+} - \mathbf{f}_-\boldsymbol{\psi}_{A-}, \tag{14}$$

and the total displacement is given by

$$\mathbf{q}_A = \boldsymbol{\zeta}_+\boldsymbol{\psi}_{A+} + \boldsymbol{\zeta}_-\boldsymbol{\psi}_{A-}. \tag{15}$$

Now, the boundary condition at A is $\mathbf{q}_A = \boldsymbol{\alpha}_A\mathbf{F}_A$, and substitution of Eqs. (14) and (15) into this finally yields a relationship between the generalized wave coordinate vectors of the reflected waves $\boldsymbol{\psi}_{A+}$ and the incident waves $\boldsymbol{\psi}_{A-}$:

$$\boldsymbol{\psi}_{A+} = -(\boldsymbol{\alpha}_A\mathbf{f}_+ + \boldsymbol{\zeta}_+)^{-1}(\boldsymbol{\alpha}_A\mathbf{f}_- + \boldsymbol{\zeta}_-)\boldsymbol{\psi}_{A-}. \tag{16}$$

In short form this reads

$$\boldsymbol{\psi}_{A+} = \mathbf{r}_A\boldsymbol{\psi}_{A-}, \tag{17}$$

where $\mathbf{r}_A$ is the reflection matrix of boundary A.

B. Matrix of direct receptances of *j*-element subsystem

An expression for the $n\times n$ direct receptance matrix of the left-hand subsystem with j elements in Fig. 6(b) will now be derived. The displacement vector $\mathbf{q}_O$ at junction O is a sum of contributions from displacement vectors associated with n positive-going and n negative-going waves. This can be expressed as

$$\mathbf{q}_O = \mathbf{q}_{O+} + \mathbf{q}_{O-} = \boldsymbol{\zeta}_+\boldsymbol{\psi}_{O+} + \boldsymbol{\zeta}_-\boldsymbol{\psi}_{O-}. \tag{18}$$

Further, the generalized wave coordinate vectors for the positive and negative-going waves at the other end of the subsystem, j junctions to the right, yield

$$\boldsymbol{\psi}_{jl+} = \mathbf{e}_d^{-j\boldsymbol{\mu}}\boldsymbol{\psi}_{O+}, \tag{19}$$

$$\boldsymbol{\psi}_{jl-} = \mathbf{e}_d^{j\boldsymbol{\mu}}\boldsymbol{\psi}_{O-}, \tag{20}$$

respectively. Here the notation $\mathbf{e}_d^{-j\boldsymbol{\mu}}$ and $\mathbf{e}_d^{j\boldsymbol{\mu}}$ represent *diagonal matrices* containing all values of $e^{-j\mu_i}$ and $e^{j\mu_i}$, respectively. By utilizing these expressions the total displacement vector $\mathbf{q}_{jl}$ at this position reads

$$\mathbf{q}_{jl} = \mathbf{q}_{jl+} + \mathbf{q}_{jl-} = \boldsymbol{\zeta}_+ \boldsymbol{\psi}_{jl+} + \boldsymbol{\zeta}_- \boldsymbol{\psi}_{jl-} = \boldsymbol{\zeta}_+ \mathbf{e}_d^{-j\boldsymbol{\mu}} \boldsymbol{\psi}_{O+} + \boldsymbol{\zeta}_- \mathbf{e}_d^{j\boldsymbol{\mu}} \boldsymbol{\psi}_{O-}. \quad (21)$$

Now, $\boldsymbol{\psi}_{O,+}$ and $\boldsymbol{\psi}_{O,-}$ are related through the reflection matrix $\mathbf{r}_A$ of boundary A given by Eq. (17) and utilizing this yields

$$\mathbf{q}_{jl} = (\boldsymbol{\zeta}_+ \mathbf{e}_d^{-j\boldsymbol{\mu}} \mathbf{r}_A + \boldsymbol{\zeta}_- \mathbf{e}_d^{j\boldsymbol{\mu}}) \boldsymbol{\psi}_{O-}. \quad (22)$$

In a similar way the corresponding force eigenvector $\mathbf{F}_{jl}$ is obtained as

$$\mathbf{F}_{jl} = \mathbf{F}_{jl+} + \mathbf{F}_{jl-} = -\mathbf{f}_+ \boldsymbol{\psi}_{jl+} - \mathbf{f}_- \boldsymbol{\psi}_{jl-} = -\mathbf{f}_+ \mathbf{e}_d^{-j\boldsymbol{\mu}} \boldsymbol{\psi}_{O+} - \mathbf{f}_- \mathbf{e}_d^{j\boldsymbol{\mu}} \boldsymbol{\psi}_{O-}, \quad (23)$$

and further use of the reflection matrix $\mathbf{r}_A$ gives

$$\mathbf{F}_{jl} = (-\mathbf{f}_+ \mathbf{e}_d^{-j\boldsymbol{\mu}} \mathbf{r}_A - \mathbf{f}_- \mathbf{e}_d^{j\boldsymbol{\mu}}) \boldsymbol{\psi}_{O-}. \quad (24)$$

Solving for $\boldsymbol{\psi}_{O,-}$ and substitution in Eq. (22) finally yields a relationship between the displacement vector $\mathbf{q}_{jl}$ and force vector $\mathbf{F}_{jl}$ at junction j,

$$\mathbf{q}_{jl} = \boldsymbol{\gamma}_{jj} \mathbf{F}_{jl}, \quad (25)$$

where the *direct* receptance matrix $\boldsymbol{\gamma}_{jj}$ of the j-element subsystem is given by

$$\boldsymbol{\gamma}_{jj} = (\boldsymbol{\zeta}_+ \mathbf{e}_d^{-j\boldsymbol{\mu}} \mathbf{r}_A + \boldsymbol{\zeta}_- \mathbf{e}_d^{j\boldsymbol{\mu}})(-\mathbf{f}_+ \mathbf{e}_d^{-j\boldsymbol{\mu}} \mathbf{r}_A - \mathbf{f}_- \mathbf{e}_d^{j\boldsymbol{\mu}})^{-1}. \quad (26)$$

C. Matrix of transfer receptances of $(N-j)$-element subsystem

Consider the subsystem with $(N-j)$ elements lying to the right of the external force discontinuity in Fig. 6(b). For this subsystem driven at j the transfer receptance matrix $\boldsymbol{\delta}_{mj}$ of junction m can be derived using a procedure similar to that above. So, the displacement vector $\mathbf{q}_{jr}$ at the excited junction j is expressed as a sum of contributions from n positive-going waves and n negative-going waves, that is,

$$\mathbf{q}_{jr} = \mathbf{q}_{jr+} + \mathbf{q}_{jr-} = \boldsymbol{\zeta}_+ \boldsymbol{\psi}_{jr+} + \boldsymbol{\zeta}_- \boldsymbol{\psi}_{jr-}, \quad (27)$$

and the total force vector $\mathbf{F}_{jr}$ at junction j reads correspondingly

$$\mathbf{F}_{jr} = \mathbf{F}_{jr+} + \mathbf{F}_{jr-} = \mathbf{f}_+ \boldsymbol{\psi}_{jr+} + \mathbf{f}_- \boldsymbol{\psi}_{jr-}. \quad (28)$$

Further, the displacement vector at junction m, that is $(m-j)$ junctions to the right, is

$$\mathbf{q}_m = \boldsymbol{\zeta}_+ \mathbf{e}_d^{-(m-j)\boldsymbol{\mu}} \boldsymbol{\psi}_{jr+} + \boldsymbol{\zeta}_- \mathbf{e}_d^{(m-j)\boldsymbol{\mu}} \boldsymbol{\psi}_{jr-}. \quad (29)$$

At boundary B, which is $(N-j)$ junctions to the right, the generalized wave coordinate vectors $\boldsymbol{\psi}_{B+}$ and $\boldsymbol{\psi}_{B-}$ of the incident and reflecting waves are given as

$$\boldsymbol{\psi}_{B+} = \mathbf{e}_d^{-(N-j)\boldsymbol{\mu}} \boldsymbol{\psi}_{jr+}, \quad \boldsymbol{\psi}_{B-} = \mathbf{e}_d^{(N-j)\boldsymbol{\mu}} \boldsymbol{\psi}_{jr-}, \quad (30)$$

respectively, and since these two vectors are related in Eq. (12) by the reflection matrix $\mathbf{r}_B$ of boundary B, the following identity is obtained:

$$\mathbf{e}_d^{(N-j)\boldsymbol{\mu}} \boldsymbol{\psi}_{jr-} = \mathbf{r}_B \mathbf{e}_d^{-(N-j)\boldsymbol{\mu}} \boldsymbol{\psi}_{jr+}. \quad (31)$$

Rearranging this gives

$$\boldsymbol{\psi}_{jr-} = \mathbf{e}_d^{-(N-j)\boldsymbol{\mu}} \mathbf{r}_B \mathbf{e}_d^{-(N-j)\boldsymbol{\mu}} \boldsymbol{\psi}_{jr+}, \quad (32)$$

which by substitution in Eqs. (28) and (29) yields

$$\mathbf{q}_m = (\boldsymbol{\zeta}_+ \mathbf{e}_d^{-(m-j)\boldsymbol{\mu}} + \boldsymbol{\zeta}_- \mathbf{e}_d^{(m-j)\boldsymbol{\mu}} \mathbf{e}_d^{-(N-j)\boldsymbol{\mu}} \mathbf{r}_B \mathbf{e}_d^{-(N-j)\boldsymbol{\mu}}) \boldsymbol{\psi}_{jr+} \quad (33)$$

and

$$\mathbf{F}_{jr} = (\mathbf{f}_+ + \mathbf{f}_- \mathbf{e}_d^{-(N-j)\boldsymbol{\mu}} \mathbf{r}_B \mathbf{e}_d^{-(N-j)\boldsymbol{\mu}}) \boldsymbol{\psi}_{jr+}, \quad (34)$$

respectively. From Eq. (34) a relation between the external force vector $\mathbf{F}_{jr}$ and $\boldsymbol{\psi}_{jr,+}$ is obtained

$$\boldsymbol{\psi}_{jr,+} = (\mathbf{f}_+ + \mathbf{f}_- \mathbf{e}_d^{-(N-j)\boldsymbol{\mu}} \mathbf{r}_B \mathbf{e}_d^{-(N-j)\boldsymbol{\mu}})^{-1} \mathbf{F}_{jr}. \quad (35)$$

Finally, substituting this into Eq. (33) gives the displacement vector $\mathbf{q}_m$ at junction m resulting from the force vector $\mathbf{F}_{jr}$ at junction j, that is

$$\mathbf{q}_m = \boldsymbol{\delta}_{mj} \mathbf{F}_{jr}, \quad (36)$$

where we have introduced the *transfer* receptance matrix $\boldsymbol{\delta}_{mj}$ of the right-hand subsystem:

$$\boldsymbol{\delta}_{mj} = (\boldsymbol{\zeta}_+ \mathbf{e}_d^{-(m-j)\boldsymbol{\mu}} + \boldsymbol{\zeta}_- \mathbf{e}_d^{(m-j)\boldsymbol{\mu}} \mathbf{e}_d^{-(N-j)\boldsymbol{\mu}} \mathbf{r}_B \mathbf{e}_d^{-(N-j)\boldsymbol{\mu}}) \times (\mathbf{f}_+ + \mathbf{f}_- \mathbf{e}_d^{-(N-j)\boldsymbol{\mu}} \mathbf{r}_B \mathbf{e}_d^{-(N-j)\boldsymbol{\mu}})^{-1}. \quad (37)$$

Thus, the corresponding *direct* receptance matrix $\boldsymbol{\delta}_{jj}$ is obtained by letting $m=j$, so that

$$\boldsymbol{\delta}_{jj} = (\boldsymbol{\zeta}_+ + \boldsymbol{\zeta}_- \mathbf{e}_d^{-(N-j)\boldsymbol{\mu}} \mathbf{r}_B \mathbf{e}_d^{-(N-j)\boldsymbol{\mu}}) \times (\mathbf{f}_+ + \mathbf{f}_- \mathbf{e}_d^{-(N-j)\boldsymbol{\mu}} \mathbf{r}_B \mathbf{e}_d^{-(N-j)\boldsymbol{\mu}})^{-1}. \quad (38)$$

D. Matrix of junction-receptances of total system

What remains is the determination of the junction-receptances of the total system in terms of the receptance matrices $\boldsymbol{\gamma}_{jj}$, $\boldsymbol{\delta}_{mj}$, and $\boldsymbol{\delta}_{jj}$ of the two subsystems. Since the two subsystems are in parallel the externally applied force vector $\mathbf{F}_j$ must be in equilibrium with the internal forces acting on the subsystems, that is, $\mathbf{F}_j = \mathbf{F}_{jl} + \mathbf{F}_{jr}$. Continuity of displacements at the excitation point furthermore yields $\mathbf{q}_j = \mathbf{q}_{jl} = \mathbf{q}_{jr}$.

Inserting Eqs. (25) and (38) into the last part of this continuity condition gives

$$\mathbf{F}_{jl} = \boldsymbol{\gamma}_{jj}^{-1} \boldsymbol{\delta}_{jj} \mathbf{F}_{jr}, \quad (39)$$

and substituting this into the stated force equilibrium condition leads to

$$\mathbf{F}_j = (\mathbf{I} + \boldsymbol{\gamma}_{jj}^{-1} \boldsymbol{\delta}_{jj}) \mathbf{F}_{jr}, \quad (40)$$

where $\mathbf{I}$ is the unity matrix. Now, $\mathbf{F}_{jr}$ can be eliminated by combining Eqs. (36) and (40), and solving for $\mathbf{q}_m$ finally gives

$$\mathbf{q}_m = \boldsymbol{\alpha}_{mj} \mathbf{F}_j, \quad (41)$$

where $\boldsymbol{\alpha}_{mj}$ is the matrix of transfer receptances of the *total* system:

$$\boldsymbol{\alpha}_{mj} = \boldsymbol{\delta}_{mj} (\mathbf{I} + \boldsymbol{\gamma}_{jj}^{-1} \boldsymbol{\delta}_{jj})^{-1}. \quad (42)$$

Substituting the expressions derived above for $\boldsymbol{\gamma}_{jj}$, $\boldsymbol{\delta}_{mj}$, and $\boldsymbol{\delta}_{jj}$ in Eq. (42) results in a rather complicated expression for the transfer receptance $\boldsymbol{\alpha}_{mj}$. Nevertheless, the solution of this can be implemented numerically and receptances have been calculated without computational difficulties for the limited number of cases studied.

FIG. 7. Experimental arrangement. Point force excitation in longitudinal direction at junction 0.

IV. RESPONSE PREDICTION AND EXPERIMENTAL VERIFICATION

Responses in all three junction coordinates of the eight-element periodic structure in Fig. 1(a) were predicted numerically using calculated propagation constants and the junction-receptances calculated from Eqs. (26), (37), (38), and (42). Since the transverse beams of each periodic element are taken to be of half-width to sustain element symmetry, the *end terminations* of the finite periodic structure are in this case also modeled as transverse beams of half-width in order to form the full-width physical beams at the ends of the structure in question. This implies that the boundary receptance matrices $\boldsymbol{\alpha}_A$ and $\boldsymbol{\alpha}_B$ are given by those of the transverse beam components as can be found in Ref. 1. Other end terminations complying with motion in the *xy* plane may readily be included.

In order to verify the theoretical model an experimental investigation was performed on a nominally identical periodic structure; Fig. 7 shows the experimental arrangement. The structure was made of acrylic, and was suspended in elastic wires so it could vibrate freely in all directions. The structure was forced at the end by an electro-dynamic vibration exciter (Brüel & Kjær Type 4809) fed by a white noise signal. A force transducer (B&K Type 8200) measured the input force and junction responses in all three motion coordinates were measured by using 2.5 g accelerometers (Brüel & Kjær Type 4393). The data acquisition and analysis were performed by a dual-channel FFT analyser (Brüel & Kjær Type 3160 C, "Pulse-System") using a frequency resolution of 1 Hz in the band from 0 to 6400 Hz.

For ease of comparison the propagation constants from Fig. 2(c) are shown in Fig. 8 with a *logarithmic* frequency axis. In the following the numerical predictions for the finite periodic structure are compared with the measured junction-mobilities.

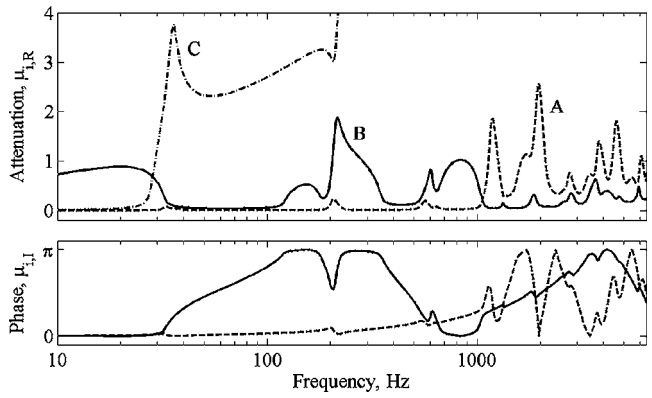

FIG. 8. Wave propagation constants; as in Fig. 2(c), but with logarithmic frequency axis.

A. Response to longitudinal (axial) force excitation

The finite periodic structure was first examined for excitation by a longitudinal force $F_0(t)$ acting at junction 0 as shown in Figs. 1 and 7. Longitudinal velocity responses $\dot{u}_j(t)$ were determined at all junctions $j=0-8$, giving the complex transfer mobilities $Y_{u,j0}=\dot{u}_j/F_0$. As examples of predicted and measured mobilities Fig. 9 shows results for junctions 0 and 8, in terms of magnitude and phase spectra. These results clearly reveal that there is a very good agreement between the predicted and measured mobilities. It is only at very low frequencies, below 50 Hz, that predicted and measured results deviate slightly. This is because the experimental structure oscillates to and through like a pendulum in its thin wire-suspensions, which were not sufficiently resilient at such low frequencies. Thus, below 50 Hz the experimental periodic structure cannot be regarded as being truly *semidefinite*, that is to say, totally *free* in space. The same phenom-

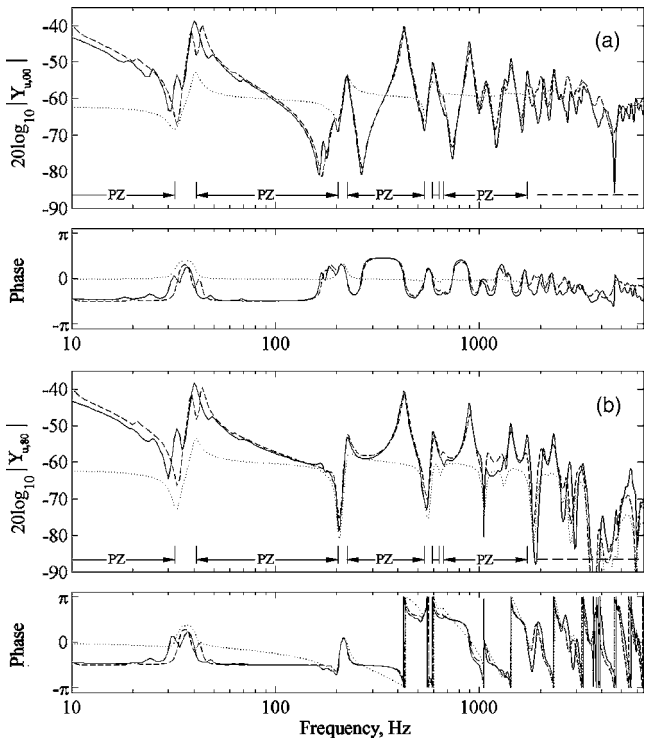

FIG. 9. Junction longitudinal mobility of finite periodic structure with eight elements; the system is driven at junction 0 by a longitudinal (axial) point force: (—) measurements; (- - -) numerical prediction using Eq. (42); (···) numerical prediction for a corresponding semi-infinite periodic structure. (a) Direct mobility $Y_{u,00}=\dot{u}_0/F_0$, and (b) transfer mobility $Y_{u,80}=\dot{u}_8/F_0$.

enon also causes calculated mobilities to be slightly higher than measured results at frequencies *below* 20 Hz, where the structure vibrates as a rigid mass, i.e., with a negative slope in magnitude and a phase of $-\pi/2$.

Also shown in Fig. 9 are calculated junction-mobilities for a corresponding, but *semi-infinite* periodic structure. By comparison with the calculated mobilities of the *finite* periodic structure, it is evident that this mostly behaves strongly resonant despite its relatively high damping loss factor. In frequency zones of sufficiently high attenuation constant μ_R, however, it is also apparent that the finite periodic structure can be treated approximately as being semi-infinite. In Fig. 9(b) this is seen around 1900 Hz and from 2800 Hz and upwards, where $\mu_R \geqslant 0.25$ and the mobilities of the semi-infinite and finite periodic structure are close to being identical. This is in agreement with the "10%-limit-condition" $N\mu_R > 1.5$ for applying the valuable semi-infinite-structure-assumption that was derived in Ref. 8 for maximum allowable response deviations of 10%, albeit for the case of mono-coupled periodic structures.

According to Sec. II and Fig. 3(c) the longitudinal motion is controlled mainly by wave-type *A* up until 1066 Hz. Thus, below this frequency, up until $N=8$ natural frequencies are expected[8,9] to occur within each propagation zone associated with wave-type *A*, provided that there is a full π-change of the phase constant μ_l. However, μ_l varies only little at frequencies below 1066 Hz because the finite periodic structure is significantly damped, and it is therefore very few of these resonances of the "eight-mode groups" that are visible in Fig. 9. The first, second, and third propagation zones, for example, lie in the bands from 0 to 32 Hz, 41 to 205 Hz, and 224 to 540 Hz, respectively. These bounding frequencies occur at the peaks and troughs in the dotted response curve for the semi-infinite structure. The peaks, which identify the *lower* bounding frequencies, correspond to the natural frequencies of a *single* periodic element when its longitudinal and rotational motion coordinates at junctions are *free* whereas transverse coordinates are *locked.* Upper bounding frequencies are identified by the troughs, which occur at the natural frequencies of an element with longitudinal and rotational junction coordinates being *locked* and transverse coordinates being *free*.[9] The mode of vibration at the lower bounding frequency of 41 Hz, for example, is strongly influenced by the transverse beams, which all vibrate in-phase virtually in their fundamental *sliding-free* mode. All junction longitudinal responses are also in-phase. The upper bound at 205 Hz is controlled by the "resonating" transverse beams vibrating in their second, virtually *clamped-free* mode. Longitudinal motions at junctions are thus virtually locked, and in the absence of damping the transverse beams will all vibrate in anti-phase with one another, because the junction-to-junction phase change is π. This influence of the transverse beams corresponds to the action of multiple dynamic neutralizer—or "absorbers". The same pattern is repeated in the next propagation zone from 224 to 540 Hz, just with increasing mode order, i.e., basically governed by the second sliding-free mode and the third clamped-free mode of the transverse beams.

Figure 10 shows calculated and measured cross mobilities $Y_{\theta,j0}=\dot{\theta}_j/F_0$ relating *rotational* velocities $\dot{\theta}_j(t)$ at junctions to the *longitudinal* driving force $F_0(t)$ at junction 0. These rotational velocities, which were measured using the finite difference from two accelerometers placed concentrically with respect to the column's neutral axis, are caused exclusively by longitudinal-flexural wave coupling in the structure. Disregarding results below 50 Hz, we find good overall agreement up until about 1200 Hz between predictions and measurements for these cross-coupled responses. Especially the peak values are almost the same at the frequencies 65, 185, 224, 420, 600, and 1100 Hz. These peaks are caused mainly by the strong longitudinal responses, which couple into rotational responses. The broadband and low-valued troughs centered around 100, 300, and 750 Hz are also in agreement. These are caused mainly by the low energy ratio of the predominantly longitudinal wave-type, that is, wave-type *A* from 0 to 1066 Hz and wave-type *B* from 1066 to 6400 Hz, see Fig. 3(c). Finally, with an overall level difference of about 5 dB the agreement is less good in the range from 1200 to 3000 Hz.

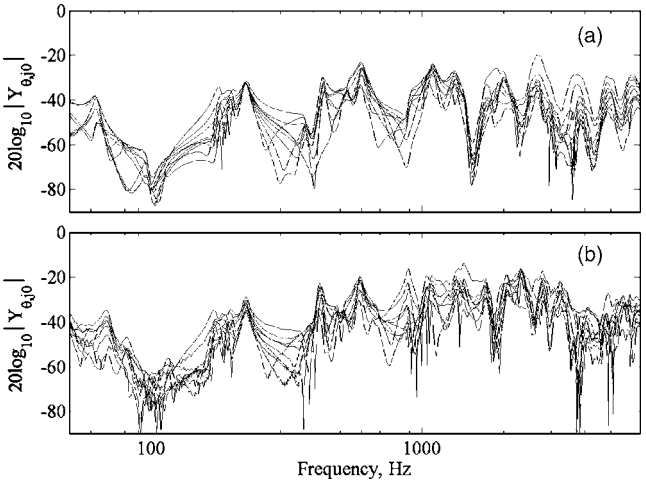

FIG. 10. Junction rotational mobilities $Y_{\theta,j0}=\dot{\theta}_j/F_0$, for $j=0-8$, of finite periodic structure with eight elements; the system is driven at junction 0 by a longitudinal point force. (a) Numerical predictions using Eq. (42), and (b) measurements.

B. Response to offset force excitation

In a second investigation the periodic structure was driven by an offset force $F_{0,\text{off}}(t)$ in order to excite primarily flexural-type waves. Figure 1 shows how the force was applied perpendicular to the first transverse beam, at a vertical distance of 183 mm from the previous driving point. This excitation resulted in a combined force and moment excitation at junction 0, of which the effect of the moment excitation was anticipated to dominate. For the prediction, this combined excitation was determined by calculating the transfer responses of the driven transverse beam and then using reciprocity between the offset point and junction 0.

For this forcing Fig. 11 shows an example of numerical predictions and measurements, in the form of junction rotational velocities per unit offset force, that is, the rotational cross mobilities $Y_{\theta,j0,\text{off}}=\dot{\theta}_j/F_{0,\text{off}}$. These single point junction mobilities are largely representative descriptors for the

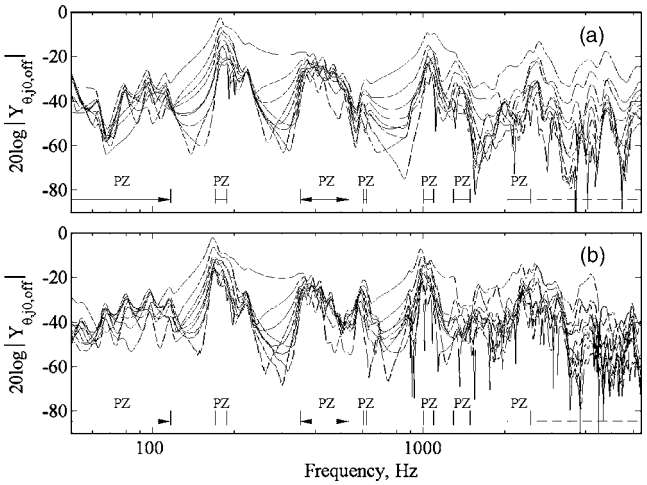

FIG. 11. Junction rotational mobilities $Y_{\theta,j0,\text{off}}=\dot{\theta}_j/F_{0,\text{off}}$, for $j=0-8$, of finite periodic structure with eight elements; the system is driven by an offset harmonic point force $F_{0,\text{off}}$ acting on the first transverse beam at 183 mm below junction 0. (a) Numerical predictions using Eq. (42), and (b) measurements.

flexural vibration in both the transverse beams and the wave-carrying column components. The responses are here seen to be governed by relatively narrow propagation zones, which are separated by strong, broadband attenuation zones. There is a fine agreement between predicted and measured results from 50 to about 1400 Hz. At the higher frequencies, however, discrepancies are noted particularly at the deep trough in the attenuation zone at about 1500 Hz. These deviations probably originate from finite-difference measurement problems associated with small rotational responses at high frequency troughs. Several moderate peaks from finite-system resonances can be observed especially in the bands from approximately 50 to 115 Hz and from 350 to 540 Hz. Furthermore, at most frequencies from 1066 Hz and upwards, where the attenuation constant of the predominantly flexural wave-type A takes values of $\mu_R \geqslant 0.35$, the vibrations are attenuated by more than 20 dB from junction 0 to junction 8. In the band from 3300 to 4800 Hz this attenuation is even 40 dB or more. This is again in accordance with the strong attenuation constant of wave-type A in Fig. 8, and this complies also with the predicted responses of the corresponding semi-infinite structure in Fig. 4(b).

Below 1066 Hz the rotational motion is expected to be controlled by the predominantly *flexural* wave-type B. However, since this wave-type is strongly attenuated in some bands, the contributions from the less attenuated and predominantly *longitudinal* wave-type A "takes over" after a few periodic elements and then dominates the transmission in the remaining parts of the periodic structure. This flexural-longitudinal wave coupling, which results in a spatially dual-rate decrease in magnitudes occurs in several narrow bands in Fig. 11, but is most clearly observed from 200 to 250 Hz and around 1200 and 2000 Hz, as is also seen in Fig. 4(b).

V. CONCLUSIONS

Periodic structure analysis has been further developed in this study of multicoupled periodic structures of both semi-infinite and finite extent. Specifically examined are propagation characteristics of flexural and longitudinal-type waves in tri-coupled periodic structures with multiresonant side-branches in the form of asymmetrically appended transverse beams. The fundamental understanding obtained for this type of transmission path is of considerable practical interest, if generalized to represent a plane-wave, normal incidence model of a similar plate assembly such as web-stiffened panels, ship hulls with decks, and floor-loaded columns in buildings.

Numerical results for semi-infinite and tri-coupled periodic systems show that the wave transmission is governed by a complicated pattern of propagation zones (passbands) for the two wave solutions which can carry energy, and that these zones are intervened by many stopbands of both moderate and high-valued attenuation. It is revealed that flexural and longitudinal motions are coupled in such systems with multiresonant side-branches, but a parameter study also shows that structural damping has a significant influence on this phenomenon. The otherwise strong coupling between flexural and longitudinal motions occurring in lightly damped structures decreases when structural damping is increased. For a tri-coupled periodic structure it is found that this damping-dependent decrease in coupling takes place at most frequencies for a damping loss factor value of, say, 0.01 or higher. This results in a separation of the wave-field into a primarily longitudinal wave-type and a primarily flexural wave-type, of which the latter is attenuated in approximately half the frequency range considered.

By relaxing the simplifying semi-infinite-structure assumption, a general expression for the junction receptances of *finite* and *multicoupled* periodic systems is derived as a generalization of the governing expression of mono-coupled periodic systems.[8] This new expression is used for predicting audio-frequency vibration responses of an eight-element, tri-coupled periodic structure to two types of point excitations applied at its end. These predictions are compared with measurements from a freely suspended and nominally identical finite test-structure. In the case of longitudinal force excitation a very good agreement is found with measured results of the longitudinal velocity responses at junctions. Moreover, a comparison with calculated responses for a corresponding, but *semi-infinite* periodic structure, shows that the finite periodic structure behaves strongly resonant in most propagation zones despite its relatively high damping loss factor of 0.056. A good correspondence is also achieved from 50 to 3000 Hz for junction *rotational* velocities caused by either the longitudinal force or a combined moment and force excitation. For the longitudinal excitation these junction rotational velocities are caused exclusively by the predominantly longitudinal wave-type and hence by the coupling between longitudinal and flexural motions. The combined moment and force excitation is found to generate strong rotational responses in a low frequency band from 80 to 400 Hz. However, at the higher frequencies the rotational responses are of the same order of magnitude as those resulting "indirectly" from pure longitudinal force excitation. Further, with the combined excitation it is found that the junction rotational velocities are controlled by a predominantly *flexural* wave-

type. However, since this wave is strongly attenuated the motion contributions from the significantly *less* attenuated and predominantly *longitudinal* wave-type "takes over" after a few periodic elements, and hence dominate the transmission and responses in the remaining parts of the periodic structure. This type of coupling is observed in narrow frequency bands for the examined structure, and this phenomenon would explain the spatially *dual-rate* exponential decrease in vibration magnitudes, observed in nominally periodic multi-story buildings.

[1]L. Friis, M. Ohlrich, "Coupling of flexural and longitudinal wave motion in a periodic structure with asymmetrically arranged transverse beams," J. Acoust. Soc. Am. **118**, 3010–3020 (2005).

[2]M. Ohlrich, "Harmonic vibration of a column structure with transverse beams," *Proceedings of the Institute of Acoustics, Spring Meeting*, Southampton, England, 1979, Paper 20.I2.

[3]K. Gösele, *Über das Schalltechnische Verhalten von Skelettbauten (Acoustic Properties of Skeleton Building Structures)*, Körperschall in Gebäuden (Ernst, Berlin 1960).

[4]D. J. Mead and S. Markus, "Coupled flexural-longitudinal wave motion in a periodic beam," J. Sound Vib. **90**, 1–24 (1983).

[5]L. Cremer and H. O. Leilich, "Zur Theorie der Biegekettenleiter" ("On theory of flexural periodic systems"), Arch. Elektr. Uebertrag. **7**, 261–270 (1953).

[6]L. Cremer, M. Heckl, and E. E. Ungar, *Structure-borne Sound* (Springer, Berlin, 1973). Translated from German, original 1967.

[7]D. J. Mead, "A general theory of harmonic wave propagation in linear periodic systems with multiple coupling," J. Sound Vib. **27**, 235–260 (1973).

[8]M. Ohlrich, "Forced vibration and wave propagation in mono-coupled periodic structures," J. Sound Vib. **107**, 411–434 (1986).

[9]D. J. Mead, "Wave propagation and natural modes in periodic systems. II. Multi-coupled systems, with and without damping," J. Sound Vib. **40**, 19–39 (1975).

[10]D. J. Mead, "Wave propagation and natural modes in periodic systems. I. Mono-coupled systems," J. Sound Vib. **40**, 1–18 (1975).

[11]G. L. Rodgers, *Dynamics of Framed Structures* (Wiley, New York, 1959).